BIOCHEMISTRY
including biophysical chemistry & molecular biology

Article

pubs.acs.org/biochemistry

Molecular Basis of the Cooperative Binding of Cu(I) and Cu(II) to the CopK Protein from *Cupriavidus metallidurans* CH34

Miriam-Rose Ash,[⊥,¶] Lee Xin Chong,[†,‡,¶] Megan J. Maher,[*,⊥,∥] Mark G. Hinds,[*,‡,§] Zhiguang Xiao,[*,†,‡] and Anthony G. Wedd[†,‡]

[†]School of Chemistry and [‡]Biomolecular Science and Biotechnology Institute, University of Melbourne, Parkville, Victoria 3010, Australia

[§]The Walter and Eliza Hall Institute of Medical Research, Parkville, Victoria 3052, Australia

[∥]Centenary Institute of Cancer Medicine and Cell Biology, Locked Bag No. 6, Newtown, NSW 2042, Australia

[⊥]School of Molecular Bioscience, University of Sydney, NSW 2006, Australia

Supporting Information

ABSTRACT: The bacterium *Cupriavidus metallidurans* CH34 is resistant to high environmental concentrations of many metal ions. Upon copper challenge, it upregulates the periplasmic protein CopK (8.3 kDa). The function of CopK in the copper resistance response is ill-defined, but CopK demonstrates an intriguing cooperativity: occupation of a high-affinity Cu^{I} binding site generates a high-affinity Cu^{II} binding site, and the high-affinity Cu^{II} binding enhances Cu^{I} binding. Native CopK and targeted variants were examined by chromatographic, spectroscopic, and X-ray crystallographic probes. Structures of two distinct forms of $Cu^{I}Cu^{II}$-CopK were defined, and structural changes associated with occupation of the Cu^{II} site were demonstrated. In solution, monomeric $Cu^{I}Cu^{II}$-CopK features the previously elucidated Cu^{I} site in Cu^{I}-CopK, formed from four S^{δ} atoms of Met28, -38, -44, and -54 (site 4S). Binding of Cu^{I} to apo-CopK induces a conformational change that releases the C-terminal β-strand from the β-sandwich structure. In turn, this allows His70 and N-terminal residues to form a large loop that includes the Cu^{II} binding site. In crystals, a polymeric form of $Cu^{I}Cu^{II}$-CopK displays a Cu^{I} site defined by the S^{δ} atoms of Met26, -38, and -54 (site 3S) and an exogenous ligand (modeled as H_2O) and a Cu^{II} site that bridges dimeric CopK molecules. The 3S Cu^{I} binding mode observed in crystals was demonstrated in solution in protein variant M44L where site 4S is disabled. The intriguing copper binding chemistry of CopK provides molecular insight into Cu^{I} transfer processes. The adaptable nature of the Cu^{I} coordination sphere in methionine-rich clusters allows copper to be relayed between clusters during transport across membranes in molecular pumps such as CusA and Ctr1.

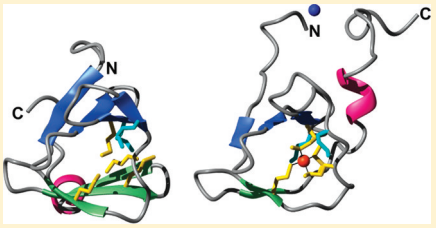

The bacterium *Cupriavidus metallidurans* CH34 is resistant to high environmental concentrations of many metal ions. It harbors two large plasmids, one of which (pMOL30) includes a *cop* cluster of at least 21 genes that respond to copper.[1,2] This cluster features the *copK* gene whose protein product CopK (8.3 kDa, 74 residues) is upregulated and exported to the periplasm upon copper challenge.[2] The function of CopK in the copper resistance response is not known, but CopK shows an intriguing copper binding cooperativity: occupation of a high-affinity Cu^{I} binding site generates a high-affinity Cu^{II} binding site, and the high-affinity Cu^{II} binding enhances the Cu^{I} binding.[3]

CopK in its apo form is a loosely associated dimer, whose dimer interface is stabilized by complementary interactions between C-terminal β-strands.[3] Each protein chain is composed of seven β-strands forming two β-sheets that sandwich a conserved methionine-rich core (see Figure 1a). With a K_D value of $\sim 10^{-5}$ M,[3,4] structural investigations in solutions with concentrations >10 μM and in crystalline phases tend to access dimer forms.

Simple dilution of apo-CopK leads to dimer dissociation but not to assembly of the high-affinity Cu^{II} site.[3] Dimer dissociation is also driven by Cu^{I} binding, but now occupation of a high-affinity methinonine-rich Cu^{I} binding site ($K_D = 2 \times 10^{-11}$ M) generates a high-affinity Cu^{II} binding site ($K_D = 3 \times 10^{-12}$ M).[3] Occupation of this Cu^{II} site, in turn, enhances Cu^{I} binding by 2 orders of magnitude.[3] There are seven methionine residues in CopK, five of which are conserved (Met26, -28, -38, -44, and -54). XANES and EXAFS data are consistent with Cu^{I} in a tetrahedral environment with four thioether ligands, and nuclear magnetic resonance (NMR) experiments on Cu^{I}-CopK detected large downfield chemical shifts for Met-C$^{\epsilon}H_3$ for four of the conserved Met side chains (Met28, -38, -44, and -54), indicating that they are the Cu^{I} ligands in solution (Figure 1b; denoted site 4S).[5] These experiments also revealed that Cu^{I} binding disrupts the C-terminal interactions, which results in dimer dissociation and reorientation of the C-terminal region

Received: June 1, 2011
Revised: September 20, 2011
Published: September 21, 2011

ACS Publications © 2011 American Chemical Society

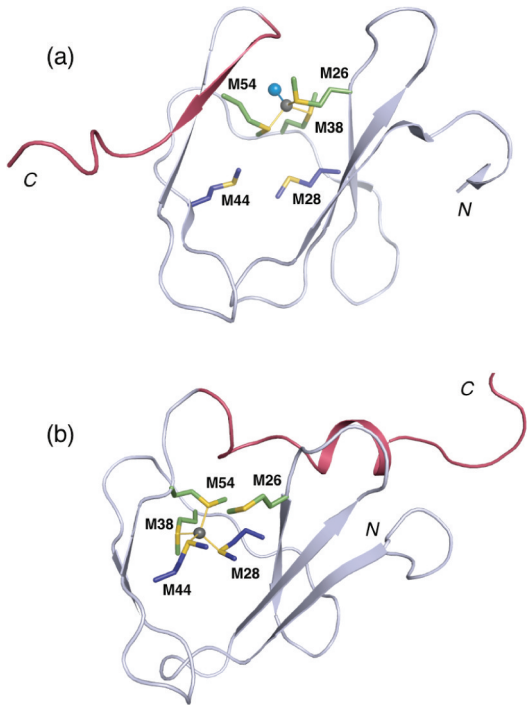

Figure 1. Comparison of the Cu^{I} sites in Cu^{I}-CopK: (a) the 3S site in the X-ray crystal structure of Cu^{I}-CopK (PDB entry 3DSO) (the structure essentially superimposes with the apo-CopK structure) and (b) the 4S site in the NMR structure of Cu^{I}-CopK (PDB entry 2KM0). Cu^{I} ligands are shown as green sticks, while the Met residues that participate only in the 4S site are shown as blue sticks. The copper atom is colored gray, and the nitrogen atom from the SCN^{-} ligand is shown as a blue sphere. The C-terminal region of residues 57−74 that reorients upon Cu^{I} binding in solution is colored pink.

via a rotation of nearly 180° around a hinge formed by Asn57 (compare panels a and b of Figure 1).[5] Attempts to crystallize $Cu^{I}Cu^{II}$-CopK led to loss of the Cu^{II} ion and crystallization of dimeric Cu^{I}-CopK, whose overall structure is very similar to that of the apo-CopK dimer.[3] Met26, -38, and -54 provide ligands for a pseudo-tetrahedral Cu^{I} site (Figure 1a; denoted site 3S), with the fourth ligand provided by NCS^{-} derived from the crystallization solution. This site shares two of the ligands (Met38 and -54) of site 4S (Figure 1a,b).

These observations in combination allowed formulation of a hypothesis that holds that there are two potential Cu^{I} binding sites (i.e., 3S and 4S) but only binding to the 4S site induces a conformational change related to generation of the high-affinity Cu^{II} site.[5] However, the molecular property associated with occupation of site 3S detected in crystals needs to be confirmed in solution, and the nature of the Cu^{II} site and the effect of its occupation on CopK remain to be defined. In this work, a set of CopK protein variants were designed and generated, aiming to address these issues. Structural (NMR and X-ray crystallography) and mutational studies indicated that the Cu^{II} binding site is formed from residues from the N- and C-terminal regions. Furthermore, a point mutation can switch high-affinity Cu^{I} binding between sites 3S and 4S, but high-affinity Cu^{II} binding enforces Cu^{I} binding at site 4S only. The solution structure of $Cu^{I}Cu^{II}$-CopK is less well ordered than those of apo- or Cu^{I}-CopK, with the Cu^{II} site lying in a disordered loop that links the N- and C-terminal residues. These observations add valuable new information about the molecular basis of the cooperative binding of Cu^{I} and Cu^{II} to the CopK protein. In addition, the versatility of the Cu^{I} coordination sphere in methionine-rich clusters displayed in CopK indicates how copper may be relayed between such clusters during transport across membranes by pumps such as CusA and Ctr1.[6]

EXPERIMENTAL PROCEDURES

Protein Chemistry. *Expression Plasmids.* Plasmid pCX07 for expression of native CopK has been described previously.[3] Plasmids for expression of CopK variants were constructed by site-directed mutagenesis on the template pCX07 plasmid via polymerase chain reaction with overlapping primers that targeted the intended mutation site. An N-terminally truncated form of CopK, $CopK_{-VDM}$, with the first three amino acids (VDM) removed, was expressed from a gene using ATG encoding the third amino acid residue Met3 as the initiation codon. An N-terminally extended CopK featuring three extra amino acids (AAA), $CopK_{+AAA}$, was expressed from a gene with codons encoding MAAA replacing those encoding the original CopK signal peptide. Each expression plasmid was confirmed by DNA sequencing.

Protein Expression, Isolation, and Characterization. Each expression plasmid was transformed into *Escherichia coli* BL21(DE3) and expressed and purified as described previously.[3] All proteins were isolated in their metal-free apo forms and their identities confirmed by ESI-MS (Table S1 of the Supporting Information). Native CopK protein was also labeled with ^{15}N and ^{13}C by culturing the expression bacterial cells in M9 minimal medium supplemented with $^{15}NH_4Cl$ and [^{13}C]glucose. ESI-MS data confirmed an average of 94% incorporation of both labels. The conformation of protein variants was assessed by examination of spectral features indicative of a folded state (e.g., downfield Hα resonances for β-strand residues and comparable methyl regions in $^{1}H-^{13}C$ HSQC spectra).

Copper-bound forms were prepared by quantitative addition of $CuSO_4$ [in the presence or absence of NH_2OH (~1 mM)] or $[Cu^{I}(CH_3CN)_4]ClO_4$ in CH_3CN to solutions of the various apo-CopK proteins in Mops buffer (20 mM, pH 6.8). Incubation was followed by gel filtration on an Econo-Pac 10DG desalting column (Bio-Rad) to remove unbound copper ions. The copper content of protein samples was determined spectrophotometrically by reaction with the Cu^{I}-specific colorimetric reagent Bcs as described previously.[7] The Cu^{I} content was determined initially and the total copper content (and hence the Cu^{II} content by difference) after subsequent addition of the reductant sodium dithionite to the same solution. Various metalated forms of CopK were also generated and analyzed using cation exchange and/or size exclusion chromatography and the copper contents analyzed as described above.

Other Biophysical Analysis. UV−visible spectra were recorded on a Varian Cary 300 spectrophotometer in dual-beam mode with quartz cuvettes with a path length of 0.5 or 1 cm. Steady-state fluorescence spectra were recorded on a Varian Cary Eclipse spectrophotometer. For fluorescence emission spectra, the excitation wavelength was 280 nm with a bandpass of 10 nm for both excitation and emission spectra. The spectra were recorded between 295 and 500 nm at a scan rate of 600 nm/min. The absorbance of protein solutions was maintained below an A_{280} of 0.1 to minimize resorption effects.

Quantitative size exclusion chromatography was conducted on a Superdex-75 gel filtration column (HR10/30, Amersham). Protein samples (1.0 mg) were applied in a volume of 0.2 mL

and eluted in Mops buffer (20 mM, pH 7.0, 100 mM NaCl) at a flow rate of 0.6 mL/min. All apo-CopK proteins (native and protein variants) eluted at the same volume, and all $Cu^{I}Cu^{II}$-CopK and $Ag^{I}Cu^{II}$-CopK proteins eluted at the same volume [see indicators (i) and (ii) in Figure 3a].

Cation exchange chromatography employed a Mono-S HR5/5 column (0.5 cm × 5 cm) equilibrated with Mops buffer (20 mM, pH 7.0). Protein samples (~100 μg) were applied, washed with buffer, and eluted with a NaCl gradient (0 to 200 mM).

NMR Spectroscopy. *Sample Preparation and Spectral Assignments.* NMR samples of native CopK protein were prepared in KP_i buffer (50 mM, pH 6.7) from ^{13}C- and ^{15}N-enriched samples. Na_2H_2EDTA (3 mM) and NaN_3 (0.04%) were included in the apo-CopK sample to remove trace metal ions and to inhibit bacterial attack. The $Cu^{I}Cu^{II}$-CopK sample was generated by reaction of apo-CopK with Cu^{2+} (2.5 equiv) in the presence of NH_2OH, followed by removal of excess Cu^{2+} on a Mono-S column. The Cu^{I}-CopK sample was obtained by quantitative anaerobic titration of EDTA-free apo-CopK with $[Cu^{I}(CD_3CN)_4]^+$ in CD_3CN (1.0 equiv). The final CD_3CN content of ~4% had a negligible influence on the spectra. The solution of $[Cu^{I}(CD_3CN)_4]^+$ in CD_3CN was prepared by dissolution of $[Cu^{I}(CH_3CN)_4]ClO_4$ in CD_3CN, followed by incubation, lyophilization, and redissolution of the solid residue in CD_3CN. NMR samples of other CopK protein variants (1.5−2.0 mM) were prepared similarly from unlabeled protein samples but with Mops buffer (20 mM, pH 6.8) substituting for KP_i buffer. CopK protein variants generally bound Cu^{I} and Cu^{II} with weaker affinities than native CopK, and the protein-bound copper ions may be partially removed by the KP_i buffer. Control experiments demonstrated that substituting KP_i for Mops buffer had a minimal effect on the chemical shifts of CopK.

NMR spectra were recorded at 25 °C on a Bruker AV-500, -600, or -800 spectrometer equipped with cryogenically cooled probes operating at 500, 600, or 800 MHz, respectively. A series of heteronuclear three-dimensional (3D) NMR experiments were recorded using doubly labeled (^{13}C and ^{15}N) native CopK protein or unlabeled CopK protein variants.[8] Spectra were processed using TOPSPIN (Bruker AG) and analyzed using XEASY.[9] Assignments were obtained for residues 7−62 and 71−74. Resonances were absent for residues 1−6 and 63−70. This represents an incompleteness of 19% of backbone assignment. Figure S1 of the Supporting Information shows the $^{1}H-^{15}N$ HSQC spectra for $Cu^{I}Cu^{II}$-CopK indicating the quality of the data that can be acquired. Some amide resonances (residues 7, 8, 10, 55, 56, and 58−62), which are absent from spectra of Cu^{I}-CopK[3] due to dynamic effects (chemical exchange, pH, or motional averaging), are present in the $^{1}H-^{15}N$ HSQC spectra of $Cu^{I}Cu^{II}$-CopK (Figure S1 of the Supporting Information). $^{1}H-^{13}C$ HSQC spectra of variant proteins were acquired at natural abundance, and assignment of methionine methyl resonances was made on the basis of the known assignments for $Cu^{I}Cu^{II}$-CopK, Cu^{I}-CopK, and apo-CopK.

Distance and Dihedral Angle Restraints. Distance restraints were measured from the 120 ms mixing time 3D ^{15}N-edited NOESY, ^{13}C-edited NOESY, and 2D NOESY spectra. Hydrogen bond constraints were applied within α-helices at a late stage of the structure calculation. Backbone torsion angles ϕ and ψ were derived using TALOS,[10] and dihedral angle restraints for ϕ and ψ angles were used as summarized in Table S2 of the Supporting Information. $^{3}J_{HNH\alpha}$ values were derived from a 3D HNHA spectrum.[11] The sequence distribution and the number of distance constraints are shown in Figure S6 of the Supporting Information.

Structure Calculation and Analysis. Initial structures were calculated using CYANA 2.1[12] and refined using XPLOR-NIH.[13] The Cu^{I} center was placed in a tetrahedral environment (site 4S) with the S^{δ} atoms of Met28, -38, -44, and -54 as ligand atoms at a $Cu-S^{\delta}$ distance of 2.3 Å and imposed tetrahedral bond angles of 109.5° (see ref 5). Ligands for a model of a square planar Cu^{II} center were chosen initially on the basis of the characterization of variant proteins indicating the amino terminus and N^{δ} of His70 as likely ligands. The carboxylate of Asp2 was added to the coordination sphere after initial calculations showed that it was nearby and could be accommodated without violations of either experimental or standard geometry (bonds, angles, and impropers). In the absence of another candidate, a water molecule was chosen as the fourth ligand to satisfy standard Cu^{II} coordination chemistry, as UV−visible absorption spectroscopy indicated that the Cu^{II} site in $Cu^{I}Cu^{II}$-CopK was a typical T2 site. Attempts at using other potential ligands (e.g., Lys69) introduced large unfavorable energy contributions. Cu−O and Cu−N bond lengths were set at 2.0 and 2.2 Å, respectively. Structural statistics for the final set of 20 structures, chosen on the basis of their stereochemical energies, are presented in Table S2 of the Supporting Information. PROCHECK_NMR[14] and MOLMOL[15] were used for the analysis of structure quality. The final structures had no experimental distance violations greater than 0.5 Å or dihedral angle violations greater than 5°.

X-ray Crystallography. *Crystal Growth and Data Collection.* Concentrated $Cu^{I}Cu^{II}$-CopK (~21 mg/mL, 10 mM KP_i, pH 6.7, 70 mM NaCl) was used for screening at room temperature using the hanging-drop vapor diffusion method with commercially available screens (Qiagen). Crystallization drops were set up in 96-well plates (Greiner Bio-One) using a Mosquito nanoliter liquid handling robot (Molecular Dimensions). Reservoir solution (200 nL) was mixed with an equal volume of a $Cu^{I}Cu^{II}$-CopK stock solution. Initial crystals of Cu^{II}_{br}-CopK were observed in condition 12 of the Classics screen [0.2 M KNO_3, 20% (w/v) PEG 3350]. The subscript br identifies Cu^{II} atoms that bridge protein dimer units. Crystal growth was optimized in larger drops (1 μL each of protein and reservoir solutions), and diffraction-quality crystals of Cu^{II}_{br}-CopK grew at room temperature from reservoir solution containing KNO_3 (0.2 M) and PEG 3350 (24%).

Initial $Cu^{I}Cu^{II}_{br}$-CopK crystals were obtained in condition 86 of the Classics screen [0.2 M ammonium acetate, 0.1 M sodium acetate, pH 4.6, 30% (w/v) PEG 4000]. However, standard optimization failed to produce diffraction-quality crystals, so a 96-condition additive screen (Hampton Research) was applied. An additive solution (500 nL) was mixed with a protein solution (2 μL) and a reservoir solution [2 μL, 0.1 M sodium acetate, 0.2 M ammonium acetate, pH 3.8, 32% (w/v) PEG 4000]. Single plates of $Cu^{I}Cu^{II}_{br}$-CopK were observed in additive condition 12 [0.1 M nickel(II) chloride].

All data were acquired on cryoprotected crystals at 100 K at GM/CA-CAT beamline 23ID-D at the Advanced Photon Source (Argonne National Laboratory, Argonne, IL) and recorded on a MAR300 CCD detector (MAR research). To positively identify copper atoms, data were collected at energies both above (9000 eV) and below (8349 eV for $Cu^{I}Cu^{II}_{br}$-CopK and 8900 eV for Cu^{II}_{br}-CopK) the Cu Kα absorption edge. The

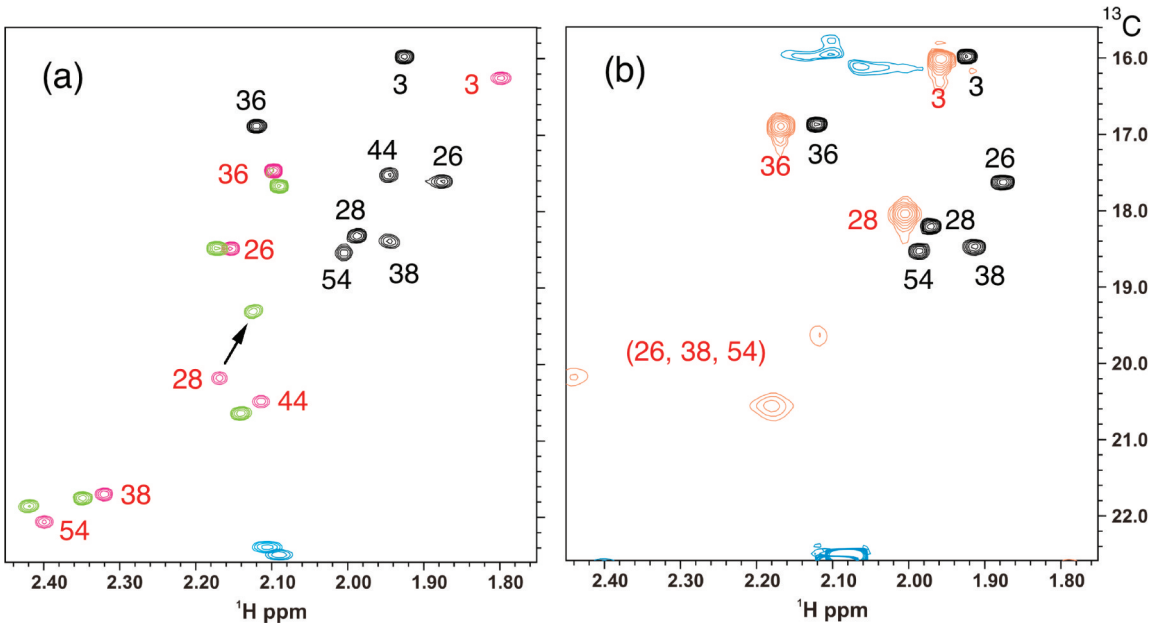

Figure 2. Identification of Cu^I-binding methionine residues using $^1H-^{13}C$ HSQC spectra at 800 MHz. Only the Met-C$^\varepsilon$ region is shown: (a) apo-CopK (black), Cu^I-CopK (red), and Cu^ICu^{II}-CopK (green), as reported previously by Sarret et al.,[5] and (b) apo-M44L (black) and Cu^I-M44L (red). Upon Cu^I binding, significant downfield shifts were observed in both the ^1H and ^{13}C dimensions for Met28, -38, -44, and -54 in wild-type CopK and Met26, -38, and -54 in M44L. Resonances from Mops are colored blue.

high-energy data sets were used for refinement. All images were processed and scaled using *HKL-2000*,[16] and a summary of data processing statistics is presented in Table S3 of the Supporting Information.

Structure Solution and Refinement. Structures were determined by molecular replacement using PHASER.[17] The high-resolution crystal structure of Cu^I-CopK (PDB entry 3DSO) was employed as a search model. All waters, Cu atoms, and the SCN^- ion were removed from the model prior to molecular replacement. Structures were refined with phenix.refine,[18] including TLS parametrization of atomic temperature factors.[19] Manual model building and the addition of waters were performed in COOT.[20] Models were validated using MolProbity,[21] SFCHECK,[22] and WHAT IF.[23] Refinement statistics for both structures are listed in Table S3 of the Supporting Information. All structural figures were prepared with PyMOL (http://www.pymol.org/).

Cu^{II}_{br}-CopK and $Cu^ICu^{II}_{br}$-CopK crystallized in space group *C*2 and contain two CopK molecules in the asymmetric unit. Refinement of Cu^{II}_{br}-CopK converged with the following residuals: R_{work} = 0.199, and R_{free} = 0.267. The final model contains residues 5−63 for chains A and B, two Cu atoms, and six water molecules. R_{work} and R_{free} values for $Cu^ICu^{II}_{br}$-CopK were 0.210 and 0.277, respectively. The model contains residues 5−63 of chain A, residues 6−21 and 25−63 of chain B, three Cu atoms, and seven water molecules. Full-length mature CopK contains 74 amino acids, and the disordered regions at the N- and C-termini of both structures represent ∼20% of the sequence.

Validation of Copper Sites. Anomalous difference Fourier maps were constructed with data collected at energies both above and below the Cu Kα absorption edge (8978.9 eV). In the maps constructed with the high-energy data, there were two peaks (of heights 28σ and 27σ) for Cu^{II}_{br}-CopK and three peaks (of heights 28σ, 19σ, and 17σ) for $Cu^ICu^{II}_{br}$-CopK. As nickel salts were present in the crystallization medium for $Cu^ICu^{II}_{br}$-CopK and the Kα absorption edge for nickel (8332.8 eV) is lower in energy than that of copper, the low-energy data were collected at the nickel edge. All peaks were absent in the map constructed with the low-energy data set, positively identifying the metal atoms as copper.

RESULTS

Generation of Protein Variants. Previous studies have identified the five Met residues (Met26, -28, -38, -44, and -54) as ligands participating in Cu^I binding at sites 3S and 4S (Figure 1).[3,5] CopK variants M44L and M54L were generated to target those sites. Residues His19, His70, Glu58, and Asp63 have been suggested as possible ligands for the high-affinity Cu^{II} binding site, and CopK point mutants H19F, H70F, E58L, and D63L were designed to examine the role of these potential Cu^{II} ligands. Previous structural studies had indicated that residues near the N-terminus may be involved in binding Cu^{II}.[3] Consequently, N-terminally truncated $CopK_{-VDM}$ (CopK with the three N-terminal residues deleted) and extended $CopK_{+AAA}$ (CopK with three additional Ala residues at the N-terminus) forms were generated to probe this possibility. The identity of each variant was confirmed by DNA sequencing and ESI-MS of the isolated protein (Table S1 of the Supporting Information). All proteins were isolated in their metal-free apo forms, and their elution positions on an analytical gel filtration column are indistinguishable from that of native apo-CopK, confirming that each variant is dimeric in solution.

Protein Variants That Affect the High-Affinity Cu^I Binding Sites. NMR experiments with apo- and Cu^I-CopK samples detected large downfield chemical shifts for Met-C$^\varepsilon$H$_3$ for four of the seven Met side chains (Met28, -38, -44, and -54) upon binding of Cu^I, which was consistent with these residues constituting the Cu^I binding site in solution [site 4S (Figure 1b)].[5] Downfield chemical shifts for Met-C$^\varepsilon$H$_3$ resonances observed for Cu^ICu^{II}-CopK were equivalent to those seen for

dx.doi.org/10.1021/bi200841f | *Biochemistry* 2011, 50, 9237−9247

Cu^I-CopK, confirming that site 4S is occupied in both forms of the protein (Figure 2a).[5]

Our earlier study demonstrated that metalation of native apo-CopK solutions (≥50 μM) is accompanied by characteristic changes in molecular properties in solution.[3] In particular, (i) the comparative elution volumes on gel filtration columns identify association states [monomer vs dimer (Figure 3a)]. (ii)

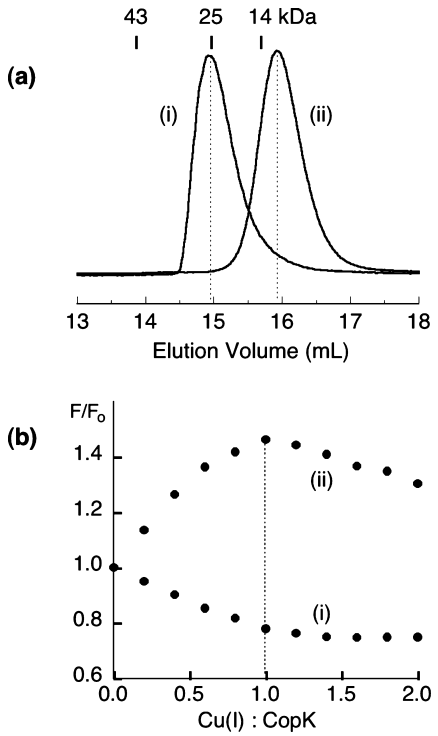

Figure 3. Experiments demonstrating different forms of Cu^I binding to various CopK variants in Mops buffer (20 mM, pH 7.0, 100 mM NaCl). (a) Size exclusion chromatographic elution profiles of (i) Cu^I-M44L (various apo-CopK proteins were eluted at the same position) and (ii) Cu^I-H70F (Cu^I-CopK$_{+AAA}$ and Cu^ICu^{II}-CopK were eluted at the same position). The elution positions of molecular standards are indicated above the chromatograms. (b) Changes in relative fluorescence emission intensity at 310 nm upon titration of $[Cu^I(CH_3CN)_4]^+$ into apoprotein solutions (50 μM) of (i) M44L and (ii) H70F (similar changes were observed for CopK$_{+AAA}$ and wild-type CopK).

Dimer dissociation following high-affinity binding of Cu^I perturbs the environment of the unique tyrosine residue Tyr10, changing its fluorescence intensity (Figure 3b). (iii) Elution profiles on a Mono-S cation exchange column are related to association states and to metal ion stoichiometry and affinity (Figure 4). (iv) Creation of a high-affinity Cu^{II} binding site leads to isolation of a stable monomeric Cu^ICu^{II}-CopK (or Ag^ICu^{II}-CopK) protein, as detected by cation exchange chromatography and confirmed by quantitative analysis for both Cu^I and Cu^{II}. These four probes allowed assessment of the ability of the variant dimeric apoproteins to bind Cu^I and then Cu^{II} (Table 1).

Met44 is a Cu^I ligand of site 4S but not of site 3S (Figure 1). Like native CopK, apo-M44L is dimeric in solution (Figure 3a). One-dimensional and $^1H-^{13}C$ HSQC NMR spectra confirm that M44L-CopK maintains its folded state: the presence of downfield α-proton resonances is indicative of β-strands, and the positions of methyl resonances in the HSQC spectra are

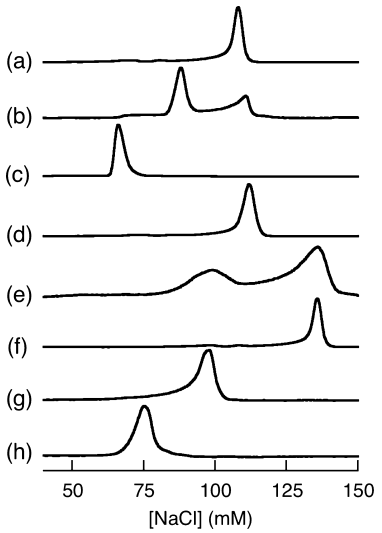

Figure 4. Cation exchange elution profiles of CopK proteins demonstrating variation of Cu^I and Cu^{II} binding and molecular states upon M44 or H70 mutation: (a) apo-CopK, (b) Cu^I-CopK (Ag^I-CopK eluted at the same position), (c) Cu^ICu^{II}-CopK (Ag^ICu^{II}-CopK eluted at the same position), (d) apo-M44L, (e) Cu^I-M44L (Cu^I bound in Cu^I-M44L is not stable and is oxidized partially during elution by air, promoted by the affinity of the Mono-S resin for the Cu^{2+} ion), (f) Ag^I-M44L, (g) apo-H70F, and (h) Cu^I-H70F.

Table 1. High-Affinity Binding of Cu^I and Cu^{II} to Dimeric Apo-CopK Proteins in Solution

protein	affinity for Cu^I	association state	affinity for Cu^{II}
wild type	high (site 4S)	monomer	high
M44L	high (site 3S)	dimer	low
M54L	low	dimer	low
H19F	lower[a] (site 3S or 4S)	dimer and monomer	high[b]
H70F	high (site 4S)	monomer	low
+AAA[c]	high (site 4S)	monomer	low
−VDM[d]	high (site 4S)	monomer	lower[a]
E58L	high (site 4S)	monomer	high
D63L	high (site 4S)	monomer	high

[a]Relative to that of the wild-type protein. [b]For the monomeric protein. [c]Three Ala residues added to the N-terminus. [d]Three residues (VDM) removed from the N-terminus.

consistent with folded protein. The natural abundance $^1H-^{15}N$ SOFAST-HMQC spectrum of apo-M44L-CopK is depicted in Figure S7 of the Supporting Information showing that the backbone amide protons have a spread of chemical shifts associated with a folded protein. The effects of titrating Cu^+ or Ag^+ into an apo-M44L solution differed markedly from those observed for native apo-CopK. (i) The products remained dimeric (Figures 3 and 4d). (ii) Copper analysis of the sole copper protein product from the gel filtration column confirmed the presence of 1 equiv of Cu^I only and the absence of Cu^{II}. (iii) As Ag^I is not susceptible to aerial oxidation, dimeric Ag^I-M44L eluted cleanly from the Mono-S cation exchange column (Figure 4d,f). In contrast, the Cu^I form underwent partial loss of metal ion upon aerobic elution (Figure 4d,e), apparently because of a combination of the high affinity of the resin for Cu^{II} and a decreased affinity of the M44L protein for Cu^I. (iv) Neither Cu^I-M44L nor Ag^I-M44L

dx.doi.org/10.1021/bi200841f | Biochemistry 2011, 50, 9237–9247

reacted with Cu^{2+} to produce isolable $Cu^{I}Cu^{II}$-M44L or $Ag^{I}Cu^{II}$-M44L, respectively.

The properties described above are consistent with those expected for dimeric forms of Cu^{I}-M44L and Ag^{I}-M44L. A $^{1}H-^{13}C$ HSQC experiment detected large downfield chemical shifts for Met-C^{ε} methyl resonances of three (Met26, -38, and -54) of the six methionine residues present in the Cu^{I}-M44L protein (Figure 2b). These three residues constitute binding site 3S defined by the X-ray structures of dimeric native Cu^{I}-CopK (Figure 1a)[3] and $Cu^{I}Cu^{II}_{br}$-CopK (as described below). The latter contains a $[Cu^{I}(S\text{-}Met)_3(OH_2)]^{+}$ site featuring aqua and Met26, -38, and -54 ligands (Figure S8 of the Supporting Information). The results indicate that mutation of Met44 to Leu disables binding at site 4S. As a consequence, Cu^{I} cannot be transferred from site 3S to site 4S and dissociation of the dimer and creation of the high-affinity Cu^{II} site are inhibited. It is apparent that the Cu^{I} binding site observed in the Cu^{I}-CopK and $Cu^{I}Cu^{II}_{br}$-CopK crystals has been reproduced in solution with the M44L-CopK protein variant.

Met54 is proposed to be a ligand of both sites 3S and 4S. Titration of Cu^{+} into the protein variant apo-M54L led to recovery of dimeric apoprotein only. As judged by criteria (i)−(iv) above, mutation of Met54 to Leu has led to the loss of high-affinity Cu^{I} binding, consistent with its assignment as a common ligand for sites 3S and 4S (Figure 1).

The potential for His19 to be a Cu^{II} ligand led to generation of the H19F-CopK variant to test its impact on high-affinity Cu^{II} binding. Unexpectedly, this mutation affected binding of Cu^{I} to the protein. Addition of 1 equiv of Cu^{+} to apo-H19F under anaerobic conditions led to an increase in fluorescence intensity, similar to that observed for native CopK (Figure 3b), signaling that Cu^{I} binding induced dimer dissociation. However, application of the reaction mixture to the cation exchange column resulted in recovery of apo-H19F-CopK, rather than the anticipated Cu^{I}-H19F species (Figure S2a,b of the Supporting Information). On the other hand, equivalent experiments with addition of excess Cu^{+} (>2 equiv) led to isolation of a dominant protein species identified as monomeric $Cu^{I}Cu^{II}$-H19F (Figure S2c of the Supporting Information). Titration of an apo-H19F-CopK solution with 1.0 equiv of Cu^{+} detected two different sets of resonances in the $^{1}H-^{13}C$ HSQC spectra, indicating the presence of two Cu^{I} species (Figure S3a of the Supporting Information). In contrast, a $^{1}H-^{13}C$ HSQC experiment with a $Cu^{I}Cu^{II}$-H19F sample isolated via size exclusion chromatography detected a single mode of binding of Cu^{I} to site 4S only (Figure S3b of the Supporting Information). We conclude that mutation of His19 to Phe has weakened the Cu^{I} affinities of both sites 3S and 4S, but differentially, one consequence being that the added Cu^{I} up to 1 equiv may equilibrate between the two sites. However, subsequent cooperative high-affinity Cu^{II} binding appears to enforce Cu^{I} binding at the site 4S only in a monomeric protein (Figure 3a and Figures S2c and S3b of the Supporting Information). As expected, sequential titration of apo-H19F-CopK with Ag^{+} and Cu^{2+} generated the stable monomeric $Ag^{I}Cu^{II}$-H19F protein.

Protein Variants That Affect the High-Affinity Cu^{II} Binding Sites. Apo-CopK exists as a weakly associated dimer in solution ($K_D \sim 10^{-5}$ M). At concentrations of $<10^{-5}$ M, the equilibrium favors the monomer. However, under such conditions, apo-CopK does not bind Cu^{II} with high affinity. The Cu^{II} ligands may be well separated in the apoprotein. A number of challenges are presented in the structural study of metalated CopK proteins in solution. The $^{1}H-^{15}N$ HSQC spectrum of Cu^{I}-CopK lacks resonances from the C-terminal region, an apparent consequence of exchange processes occurring on an intermediate chemical shift time scale.[3] This aspect is complicated further by the fact that binding of paramagnetic Cu^{II} to Cu^{I}-CopK bleaches side chain resonances.[24] In particular, residues V1−V6 of the N-terminal region and D63−H70 of the C-terminal region in the spectrum of $Cu^{I}Cu^{II}$-CopK. Absorbance and EPR spectra of the $Cu^{I}Cu^{II}$-CopK samples in solution suggested the presence of a type 2 Cu^{II} center with superhyperfine coupling to at least one ^{14}N ligand, most likely derived from His19, His70, or the N-terminus.[3] The combined influence of exchange and paramagnetic broadening demanded the application of site-directed mutagenesis to assist in the identification of the high-affinity Cu^{II} binding site.

The amide resonance of His70 is apparent in NMR spectra of Cu^{I}-CopK (BMRB entry 16408)[5] but could not be detected in a $^{1}H-^{15}N$ HSQC spectrum of native $Cu^{I}Cu^{II}$-CopK, suggesting indirectly that it may be a Cu^{II} ligand.[3] Titration of Cu^{+} into an apo-H70F-CopK solution reproduced all the characteristics typical of high-affinity Cu^{I} binding at site 4S (Figures 3 and 4g,h). The sole protein product contained 1 equiv of Cu^{I} only, confirming its identity as stable monomeric Cu^{I}-H70F. It did not react with Cu^{2+} further, demonstrating that His70 in the C-terminal region plays an essential role in high-affinity Cu^{II} binding. Unlike the Cu^{I} sites, the potential Cu^{II} ligands are not strongly conserved positionally, although all CopK sequences bear a C-terminal His residue.[3]

As discussed above, mutation of His19 to Phe weakens Cu^{I} binding on sites 3S and 4S differentially such that the added Cu^{I} seems to be equilibrated between the two sites (Figure S3a of the Supporting Information). However, the protein can bind 1 equiv of Cu^{II} further with high affinity, and this enforces all Cu^{I} to bind at site 4S only, producing stable monomeric $Cu^{I}Cu^{II}$-H19F species (Figures S2c and S3b of the Supporting Information). Consequently, His19 does not contribute significantly to high-affinity Cu^{II} binding. It is not highly conserved in CopK proteins.[3]

N-Terminally truncated $CopK_{-VDM}$ and extended $CopK_{+AAA}$ variant forms provided further revealing information. The Cu^{I} and Cu^{II} binding characteristics of $CopK_{+AAA}$ are very similar to those of H70F (Table 1 and Figures 3 and 4g,h), suggesting the N-terminus and/or Asp2 as a second Cu^{II} binding ligand. Interestingly, the truncated form $CopK_{-VDM}$ can still bind both Cu^{I} and Cu^{II} to produce isolable monomeric $Cu^{I}Cu^{II}$-$CopK_{-VDM}$ protein. However, its Cu^{II} binding affinity is more than 10 times weaker than that of the native protein, $Cu^{I}Cu^{II}$-CopK, as demonstrated by the following experiments. Like native CopK,[3] $CopK_{-VDM}$ also reacts sequentially with $AgNO_3$ and $CuSO_4$ to produce isolable monomeric products Ag^{I}-$CopK_{-VDM}$ and $Ag^{I}Cu^{II}$-$CopK_{-VDM}$ by elution from an analytical cation exchange column (Figure 5a,b). Reaction of $Ag^{I}Cu^{II}$-$CopK_{-VDM}$ and Ag^{I}-CopK in a 1:1 molar ratio, followed by analysis of the reaction mixture on the cation exchange column, revealed partial transfer of Cu^{II} ion from the former species to the latter species (Figure 5d):

$$Ag^{I}Cu^{II}\text{-}CopK_{-VDM} + Ag^{I}\text{-}CopK \rightleftharpoons Ag^{I}\text{-}CopK_{-VDM} + Ag^{I}Cu^{II}\text{-}CopK \quad (1)$$

With reference to a control elution of equimolar $Ag^{I}Cu^{II}$-CopK protein only (red dashed line in Figure 5d), the well-separated protein peak for product $Ag^{I}Cu^{II}$-CopK that eluted at the same

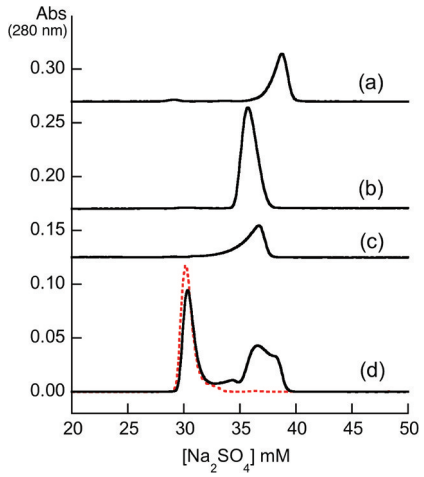

Figure 5. Cation exchange elution profiles demonstrating a weaker Cu^{II} affinity in $CopK_{-VDM}$. Equivalent masses of protein (~100 μg) were used in all experiments. The intensities were monitored at 280 nm and were not normalized. The molar extinction coefficients at 280 nm of Cu^{II}-containing proteins are more than double those of the corresponding Cu^{II}-free forms. Traces a–c have been displaced for the sake of clarity: (a) Ag^{I}-$CopK_{-VDM}$, (b) $Ag^{I}Cu^{II}$-$CopK_{-VDM}$, (c) Ag^{I}-CopK, and (d) $Ag^{I}Cu^{II}$-CopK (red dashed line). The black solid line shows the trace for an equimolar reaction mixture of $Ag^{I}Cu^{II}$-$CopK_{-VDM}$ (b) and Ag^{I}-CopK (c). An essentially superimposed elution profile was observed for an equimolar reaction mixture of Ag^{I}-$CopK_{-VDM}$ and $Ag^{I}Cu^{II}$-CopK (see eq 1). The integrated intensity of the first elution peak for $Ag^{I}Cu^{II}$-CopK was ~80% of that of the control elution of equimolar $Ag^{I}Cu^{II}$-CopK, shown as the red dashed line.

position allowed an estimation of ~80% of Cu^{II} transfer in the reaction. This estimates an exchange constant of ~16 for eq 1; i.e., the Cu^{II} affinity in Ag^{I}-CopK is ~16 times stronger than that in Ag^{I}-$CopK_{-VDM}$. On the other hand, <20% of Cu^{II} transfer was observed in the reverse reaction of eq 1 between Ag^{I}-$CopK_{-VMD}$ and $Ag^{I}Cu^{II}$-CopK, further confirming the difference in Cu^{II} affinity between the two protein species.

These results indicate that one Cu^{II} ligand (His70) originates from the C-terminal region of residues 57–74, consistent with the fact that a translation of the latter upon Cu^{I} binding is essential for cooperative assembly of the Cu^{II} site (Figure 1). The fact that the N-terminal region provides at least one Cu^{II} ligand (N-terminus and/or Asp2) supports this analysis.

Attempts to identify additional Cu^{II} ligands were unsuccessful. Other potential Cu^{II} ligands such as Glu58 and Asp63 were also mutated, as their HN resonances were not detected in the $^{1}H-^{15}N$ HSQC spectrum of $Cu^{I}Cu^{II}$-CopK. However, mutation of either residue to Leu had little effect on the overall Cu^{I} and Cu^{II} binding character of the CopK protein (data not shown), consistent with these residues not being involved directly in high-affinity Cu^{II} binding.

Solution Structure of $Cu^{I}Cu^{II}$-CopK. Backbone superposition of the 20 structures derived for $Cu^{I}Cu^{II}$-CopK is shown in Figure 6. Residues 1–6 and 62–74 in the N- and C-terminal regions are disordered. A comparison of the apo, Cu^{I}, and $Cu^{I}Cu^{II}$ structures in solution is displayed in Figure 7. $Cu^{I}Cu^{II}$-CopK features two short antiparallel β-sheets, consisting of two and three strands (β1, residues 10 and 11; β2, residues 17 and 18; β3, residues 28 and 29; β4, residues 44 and 45; β5, residues 51 and 52; strands numbered as for the apo-CopK structure) and a turn of 3:10 helix ($\alpha_{3:10}$, residues

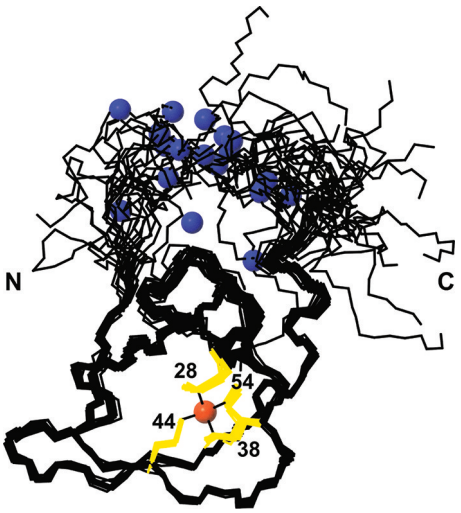

Figure 6. Solution structure of $Cu^{I}Cu^{II}$-CopK. Backbone (N, Cα, and C′) superposition of the 20 NMR-derived structures of $Cu^{I}Cu^{II}$-CopK over residues 8–61. Methionine side chains forming the Cu^{I} binding site are colored yellow, and the Cu^{I} ion is colored orange. The Cu^{II} site exists in a disordered region and links the N- and C-terminal regions. The Cu^{II} center is colored blue. N and C denote the N- and C-termini, respectively, and the Cu^{I} binding methionines are numbered.

59–62). A small hydrophobic core is formed by the side chains of conserved residues Met28, -44, and -54 projecting from the β-strands with Met38 located in the β3–β4 interstrand loop. Apart from Met3 and Met36, the methionine residues are buried, and this methionine-rich core also defines the Cu^{I} binding site. The metal ion occupies the solvent inaccessible tetrahedral 4S site provided by the S^{δ} atoms of Met28, -38, -44, and -54 (Figure 6). The methyl resonances of these conserved residues of $Cu^{I}Cu^{II}$-CopK are shifted downfield of their positions in the $^{1}H-^{13}C$ HSQC spectrum in apo-CopK (Figure 2a).[5] Resonances of the structural core are not highly perturbed by the presence of Cu^{II}, indicating that the paramagnetic ion is ≥11 Å from these residues.

While the Cu^{I} site occupies a well-ordered region, the Cu^{II} ligands are located in unstructured regions of the N- and C-termini. Results discussed in the previous section identify H70 in the C-terminal region as a likely ligand. In addition, the resonance for Met3-$C^{\epsilon}H_3$, while detected in the apo and Cu^{I} forms, is absent from the $^{1}H-^{13}C$ HSQC spectrum of $Cu^{I}Cu^{II}$-CopK (Figure 2a), consistent with its proximity to the paramagnetic Cu^{II} center. The observations suggest the presence of a ligand(s) close to the N-terminus. In fact, resonances for residues 1–6 and 63–74 are all absent, apparently because of their proximity to the paramagnetic Cu^{II} ion. This further documents the likelihood of Cu^{II} ligands being provided by both the N- and C-termini. A square planar Cu^{II} site was modeled using the N-terminal amine and His70 to form a loop. Asp2 was added as another ligand without an energetic penalty. The fourth ligand was modeled as water, because of the absence of a suitable proximal candidate among residues 1–6 and 63–74. Attempts to use other residues (such as Lys69) led to energetically unfavorable structures. A summary of restraints and structural statistics for the 20 lowest-energy structures of $Cu^{I}Cu^{II}$-CopK is given in Table S2 of the Supporting Information.

The most notable structural difference between the apo and copper-bound forms of CopK [solved here or by Sarret et al.

dx.doi.org/10.1021/bi200841f | Biochemistry 2011, 50, 9237–9247

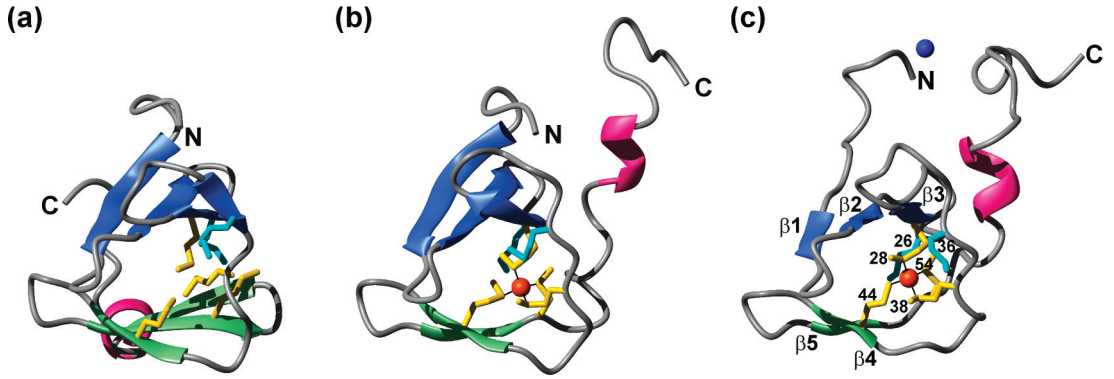

Figure 7. Solution structures of CopK showing the Cu^{I} site: (a) apo-CopK (PDB entry 2K0Q), (b) Cu^{I}-CopK (PDB entry 2KM0), and (c) $Cu^{I}Cu^{II}$-CopK. Side chains of Cu^{I}-ligating methionines (Met28, -38, -44, and -54) are colored yellow and side chains of Met26 and -36 cyan. The Cu^{I} ion is colored orange and the Cu^{II} ion blue. The orientation shown is the same as that in Figure 6.

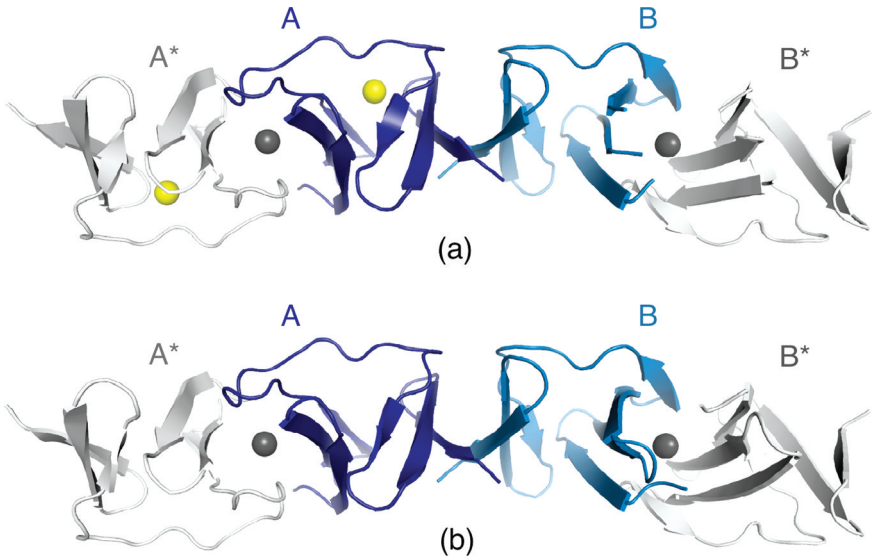

Figure 8. Positions of Cu sites in (a) $Cu^{I}Cu^{II}_{br}$-CopK and (b) Cu^{II}_{br}-CopK. The asymmetric unit is colored blue, and symmetry-related molecules are colored gray. Cu^{II} atoms are shown as dark gray spheres, and Cu^{I} atoms are shown as yellow spheres. The Cu^{II} site I exists between chains A and A*, while site II exists between chains B and B*.

(PDB entry 2KM0[5])] is the loss of the C-terminal strand of the β-sandwich upon binding of Cu^{I}. The decreased order in $Cu^{I}Cu^{II}$-CopK is reflected in the chemical shift index plot (Figure S5 of the Supporting Information); fewer Hα and Cα resonances appear in ordered regions (i.e., three or more consecutive residues with the same index) of the CSI plot when compared to that of apo-CopK.

Cu^{I} Site in Crystalline $Cu^{I}Cu^{II}_{br}$-CopK. Previous attempts to crystallize $Cu^{I}Cu^{II}$-CopK produced crystals of dimeric Cu^{I}-CopK whose structure essentially superimposes on that of apo-CopK with Cu^{I} occupying site 3S (Figure 1a).[3] Further crystallization attempts in this work under different conditions using the same isolated monomeric $Cu^{I}Cu^{II}$-CopK led to crystallization of two polymeric forms, Cu^{II}_{br}-CopK and $Cu^{I}Cu^{II}_{br}$-CopK. Both structures contain Cu^{II} that bridges adjacent protamers and mediates crystal packing. These copper sites are designated br for bridging in the Cu^{II}_{br}-CopK and $Cu^{I}Cu^{II}_{br}$-CopK notation employed here. Both Cu^{II}_{br}-CopK and $Cu^{I}Cu^{II}_{br}$-CopK crystallized with dimers in the asymmetric unit (protomer chains labeled A and B in Figure 8). The dimer interface is equivalent to that observed for apo-CopK and Cu^{I}-CopK described previously[3] and is formed from intermolecular interactions between terminal β-strands [residues 59−63 (Figure S4 of the Supporting Information)].

In $Cu^{I}Cu^{II}_{br}$-CopK, a Cu^{I} atom in site 3S present in chain A only. It is bound by the side chains Met26, -38, and -54 [Cu−S^{δ} distances of 2.6, 2.5, and 2.6 Å (Figure 8 and Figure S8a of the Supporting Information)]. Structure refinement showed a sphere of residual positive $F_O - F_C$ electron density adjacent to the copper atom that was modeled as a water molecule (Cu−O distance of 2.1 Å). This 3S site is similar to that observed in crystalline Cu^{I}-CopK where the fourth ligand is supplied by NCS^{-}, a component of the crystallization medium.[3] A search of the Cambridge Structural Database (CSD) failed to locate any three-coordinate $Cu^{I}(SR_2)_3$ centers. However, there were two structures with tetrahedral four-coordinate geometry containing three thioether ligands and an oxygen atom as the fourth ligand.[25,26] The oxidation state of the copper in the crystal structure of Cu^{I}-CopK was confirmed as 1+ by a scan of the copper absorption edge.[3] Hence, the equivalent site in our $Cu^{I}Cu^{II}_{br}$-CopK structure has been assigned as $[Cu^{I}(S\text{-}Met)_3(OH_2)]^{+}$. The assignment is consistent with the presence of soft ligands for Cu^{I} and confirms the essential nature of the 3S Cu^{I} site (Figure 1a).

An overlay of the methionine ligands in their apo and Cu^I-bound conformations is shown in Figure S8b of the Supporting Information. In the apo crystals, Met38 projects into the binding pocket while Met54 is oriented away from the binding site and is hydrogen bonded to the backbone amide of residue Asn57. This hydrogen bond has an S^{δ}−N distance of 3.3 Å, which is typical for weak hydrogen bonds of this type.[27] The binding of Cu^I to form site 3S induces structural rearrangement of Met38 and Met54. Met38 is shifted out of the site to accommodate the metal, while Met54 reorients toward it. The movement of Met54 involves breakage of the S^{δ}−N hydrogen bond that is present in the apo rotamer. The orientation of Met26, the third ligand, is the same in its apo and holo states.

Site 3S is occupied only in chain A, and the equivalent site in chain B is empty (Figure 8a), suggesting an inherent selectivity in crystal packing. Superposition of Cu^I-bound chain A onto apo-chain B shows only one region of significant difference in their C_α positions. This region (residues 35−40) has a root-mean-square deviation of 2.5 Å and includes residue Met38, one of the three Cu^I ligands. In the absence of Cu^I, the protein backbone and the side chain of M38 shift inward and project into the Cu^I binding site. The two possible backbone conformations of this region can thus be defined according to the metalated state: the holo conformation when Cu^I is bound and the backbone is away from the binding site and the apo conformation when the Cu^I site is empty and the backbone projects into the binding site.

Copper(II) Sites in Crystalline Cu^{II}_{br}-CopK and $Cu^ICu^{II}_{br}$-CopK. Both $Cu^ICu^{II}_{br}$-CopK and Cu^{II}_{br}-CopK contain bridging Cu^{II} ions. In each structure, the two Cu^{II} atoms lie on crystallographic 2-fold rotational symmetry axes and are bound to neighboring CopK asymmetric units at sites distal to the dimer interface (Figure S9 of the Supporting Information). One Cu^{II} ion is bound to chains A and A* (site I) while the second to chains B and B* (site II). Molecules A* and B* are related to the asymmetric unit by symmetry operations $-x - 1$, y, $-z$ and $-x + 1$, y, $-z + 1$, respectively. The copper atoms bridge adjacent asymmetric units and mediate crystal packing. As they lie on a 2-fold axis, they each were assigned a fractional occupancy of 0.5, generating two fully occupied copper sites upon application of the relevant rotational symmetry operators.

Cu^{II} sites I and II in each structure (Figure 8) may be assigned to a center *trans*-$[Cu^{II}(N\text{-}His)_2(O\text{-}Glu)_2]$ with His19, His19*, Glu29, and Glu29* providing a distorted square planar site with hard ligands (Figure S9 of the Supporting Information). Although this is the first CopK Cu^{II} site to be characterized structurally in the solid state, it should be noted that, while Glu29 is conserved fully in all CopK homologues, His19 is partially conserved only.[3] Low-affinity Cu^{II} sites ($K_D > 10^{-6}$ M) exist in both monomeric and dimeric forms in solution, and it is possible that His19 is a contributing ligand for weak binding.[3] However, these weak bridging Cu^{II} sites differ distinctly from the high-affinity Cu^{II} site generated upon Cu^I binding at site 4S, highlighting protein conformation-dependent Cu^I and Cu^{II} locations in the monomeric CopK protein.

DISCUSSION

Nature of the High-Affinity Cu^I Binding Sites. CopK exhibits two neighboring high-affinity Cu^I binding sites, 3S and 4S (Figure 1). Met38 and Met54 are ligands shared by these sites. Because of both the steric consequences of sharing ligands and the potential destabilization induced by cation repulsion in adjacent sites with neutral ligands, only a single site (either 3S or 4S) may be occupied at any given time. Cu^I binding at site 3S induces little overall structural change, whereas Cu^I binding at site 4S causes major structural change with rotation of the C-terminus, dissociation of the protein dimer, and creation of a high-affinity Cu^{II} binding site. In the solution state, Cu^I binds preferentially at site 4S. In crystalline forms, however, dimeric interactions are favored because of high protein concentrations and/or crystal packing, imposing the apo-CopK conformation with Cu^I being forced to occupy site 3S. Alternatively, point mutation and high-affinity Cu^{II} binding may alter the relative affinity of Cu^I binding at sites 3S and 4S, as seen for protein variants M44L and H19F.

Site 3S in apo-CopK is positioned to bind Cu^I without major structural change, but occupation of site 4S is possible only with the structural change. Notably, the shared ligand Met54 is located on a strand of the C-terminal β-sheet that contributes importantly to the dimer interface in apo-CopK. Coordination of Cu^I to this ligand at site 4S appears to play a major role in triggering the large structural change with consequent disruption of the C-terminal dimer interface and β-sheet structure. The energy required for such major structural change must arise from the free energy of Cu^I binding. Although the experimental value of K_D, 2×10^{-11} M, for site 4S in Cu^I-CopK[3] suggests that >60 kJ/mol is available overall, it is only the difference in Cu^I affinities between sites 3S and 4S that is available for construction of the Cu^{II} binding site, i.e., the difference associated with the transformation from $[Cu^I(S\text{-}Met)_3(OH_2)]^+$ to $[Cu^I(S\text{-}Met)_4]^+$. Consequently, the preference of Cu^I binding between sites 3S and 4S is modulated sensitively by a number of factors such as high-affinity Cu^{II} binding, enhanced dimer interaction, and different point residue mutations.

Nature of the High-Affinity Cu^{II} Binding Site. In the structures of apo-CopK or crystalline Cu^I-CopK dimers, His70 and the N-terminus are well-separated (Figure 1a) and neither binds Cu^{II} with high affinity. Identification of the N-terminal region and His70 side chain as the key components of the high-affinity Cu^{II} binding site allows rationalization of two other observations. (i) Apo-CopK does not bind Cu^{II} with high affinity, either in the dimer form favored at higher concentrations (>10^{-5} M) or in the monomer form favored at lower concentrations (<10^{-5} M). Dimer dissociation alone does not lead to the structural change required for the assembly of the high-affinity Cu^{II} site. (ii) High-affinity Cu^{II} binding is associated with and enhances Cu^I binding at site 4S but not at site 3S. Only Cu^I binding at site 4S can induce rotation of the C-terminus and create the high-affinity Cu^{II} binding site (Figures 1 and 7).

Molecular Basis of Cooperative Binding of Cu^I and Cu^{II}. As discussed above, the free energy of high-affinity binding of Cu^I to apo-CopK drives the cooperativity, generating the conformational change necessary to create the Cu^{II} binding site. In the process, the structure becomes less ordered overall. While a detailed mechanistic explanation is beyond the work presented here, the major structural change in the orientation of the C-terminus, based at hinge residue Asn57 with loss of a β-strand of the β-sandwich structure, as observed by us and others,[5] allows assembly of the high-affinity Cu^{II} site that incorporates His70 and other ligand(s) at the N-terminus (Figure 7).

Reorientation of the C-terminus induces dimer dissociation, occurring as a result of loss of contacts across the dimer

interface that involves the C-terminal region. When the transfer of Cu^{I} from site 3S to 4S is suppressed (e.g., in the M44L variant), the copper ion is locked at site 3S and is unable to induce the major change in protein conformation required for Cu^{II} binding. On the other hand, high-affinity Cu^{II} binding imposes a structural change that promotes the transfer of Cu^{I} from site 3S to site 4S, as seen for the copper binding chemistry of the H19F variant.

Implications for Biological Function and Copper Transport. The versatile coordination chemistry of Cu^{I} (bis, tris, or tetra coordination) aids in Cu^{I} binding and transport in biological systems. While cysteine side chains dominate binding of Cu^{I} in the cytosol,[28] methionine ligands play important roles in the more oxidizing environments of mammalian cell membranes and bacterial periplasms.[29] Well-documented examples include the soluble periplasmic proteins CusF and PcoC/CopC and the membrane Cu^{I} transporters CusA and Ctr1.[6,29]

The protein conformation-dependent Cu^{I} location in CopK provides interesting insights into the mechanism of transfer of Cu^{I} across Met-rich metal channel proteins such as CusA and Ctr1. The trimeric membrane protein CusA binds Cu^{I} at a three-methionine cluster in its periplasmic domain.[30,31] The binding is proposed to induce a conformational change that promotes transport of Cu^{I} across the membrane via a central pore. There are eight additional sets of paired methionine residues that are essential to metal ion transport and appear to bind and relay the metal ion through the inner membrane. Similarly, the eukaryotic copper transporter Ctr1 appears to translocate Cu^{I} into the cell via a series of methionine-rich sites. Like CusA, Ctr1 forms a trimeric membrane pore and bears a series of MxxM and MxM motifs that are proposed to bind and transport Cu^{I} through the pore.[6,32−34] However, an atomic-level structure of the Ctr1 transporter is not available currently, and the mechanism by which the methionine triads translocate Cu(I) is not known.

The knowledge now available from the multiple structures of CopK allows some interesting parallels to be drawn with copper transfer reactions involving methionine-rich clusters such as those in the CusA and Ctr1 systems. The CopK structures provide the first snapshots of distinct states sampled during Cu^{I} binding and transfer by methionine residues. The initial Cu^{I} binding event at site 3S, captured in the structures of crystalline Cu^{I}-CopK and $Cu^{I}Cu^{II}_{br}$-CopK, requires little movement of the relevant methionine side chains (Met26, -38, and -54). However, this initial encounter complex places the side chain of Met54 further into the protein core where it then needs to rotate only slightly to coordinate Cu^{I} in the final 4S site. This transfer of the copper into the protein core is accompanied by rearrangement of Met38, whose S^{δ} atom moves approximately 7 Å to its final Cu^{I}-bound conformation. In this way, the transfer of copper between adjacent sites is mediated not only by the adaptable nature of the Cu^{I} coordination sphere but also by the multiple degrees of freedom accessible to the methionine side chain. This unique feature further rationalizes the prevalence of methionine residues in copper translocation systems such as Ctr1 and CusA. It appears that the structural snapshots of the small CopK protein, captured at different stages of copper binding and transfer, provide a simple model for copper shuttling by methionine-rich clusters.

■ ASSOCIATED CONTENT

Ⓢ Supporting Information

Tables S1−S3 and Figures S1−S9. Experimental constraints and atomic coordinates for $Cu^{I}Cu^{II}$-CopK have been deposited in the Protein Data Bank with accession code 2LEL. Resonance assignments for $Cu^{I}Cu^{II}$-CopK have been deposited in BioMagResBank with accession code 17716. Atomic coordinates for Cu^{II}br-CopK and $Cu^{I}Cu^{II}$br-CopK have been deposited in the Protein Data Bank with accession codes 3N7E and 3N7D respectively. This material is available free of charge via the Internet at http://pubs.acs.org.

■ AUTHOR INFORMATION

Corresponding Author

*Z.X.: e-mail, z.xiao@unimelb.edu.au; fax, +61 3 9347 5180; phone, +61 3 8344 2377. M.J.M.: e-mail, m.maher@centenary.org.au; fax, +61 2 9565 6101; phone, +61 2 9565 6280. M.G.H.: e-mail, mhinds@wehi.edu.au; fax, +61 3 9347 0852; phone, +61 3 9345 2555.

Author Contributions

¶M.-R.A. and L.X.C. contributed equally to this work.

Funding

We thank the Australian Research Council for financial support (Grant A29930204).

■ ACKNOWLEDGMENTS

NMR spectra were acquired at the Bio21 Institute NMR facility, University of Melbourne.

■ ABBREVIATIONS

Bcs, bathocuproïne disulfonate anion; br, Cu^{II} atoms that bridge protein dimer units; EDTA, ethylenediamine-*N*,*N*,*N*′,*N*′-tetraacetic acid; ESI-MS, electrospray ionization mass spectrometry; HSQC, heteronuclear single-quantum coherence; IPTG, isopropyl *β*-D-thiogalactopyranoside; KP_i, potassium phosphate buffer; Mes, 2-(*N*-morpholino)ethanesulfonic acid; Mops, 3-(*N*-morpholino)propanesulfonic acid; NOESY, nuclear Overhauser spectroscopy; PDB, Protein Data Bank; XANES, X-ray absorption near edge structure.

■ REFERENCES

(1) Mergeay, M., Monchy, S., Vallaeys, T., Auquier, V., Benotmane, A., Bertin, P., Taghavi, S., Dunn, J., van der Lelie, D., and Wattiez, R. (2003) *Ralstonia metallidurans*, a bacterium specifically adapted to toxic metals: Towards a catalogue of metal-responsive genes. *FEMS Microbiol. Rev. 27*, 385−410.

(2) Monchy, S., Benotmane, M. A., Wattiez, R., van Aelst, S., Auquier, V., Borremans, B., Mergeay, M., Taghavi, S., van der Lelie, D., and Vallaeys, T. (2006) Transcriptomic and proteomic analyses of the pMOL30-encoded copper resistance in *Cupriavidus metallidurans* strain CH34. *Microbiology 152*, 1765−1776.

(3) Chong, L. X., Ash, M. R., Maher, M. J., Hinds, M. G., Xiao, Z., and Wedd, A. G. (2009) Unprecedented binding cooperativity between Cu(I) and Cu(II) in the copper resistance protein CopK from *Cupriavidus metallidurans* CH34: Implications from structural studies by NMR spectroscopy and X-ray crystallography. *J. Am. Chem. Soc. 131*, 3549−3564.

(4) Bersch, B., Favier, A., Schanda, P., van Aelst, S., Vallaeys, T., Covès, J., Mergeay, M., and Wattiez, R. (2008) Molecular structure and metal-binding properties of the periplasmic CopK protein expressed in *Cupriavidus metallidurans* CH34 during copper challenge. *J. Mol. Biol. 380*, 386−403.

(5) Sarret, G., Favier, A., Coves, J., Hazemann, J. L., Mergeay, M., and Bersch, B. (2010) CopK from *Cupriavidus metallidurans* CH34

Binds Cu(I) in a Tetrathioether Site: Characterization by X-ray Absorption and NMR Spectroscopy. *J. Am. Chem. Soc. 132*, 3770−3777.

(6) Schushan, M., Barkan, Y., Haliloglu, T., and Ben-Tal, N. (2010) Cα-trace model of the transmembrane domain of human copper transporter 1, motion and functional implications. *Proc. Natl. Acad. Sci. U.S.A. 107*, 10908−10913.

(7) Zhang, L., Koay, M., Maher, M. J., Xiao, Z., and Wedd, A. G. (2006) Intermolecular transfer of copper ions from the CopC protein of *Pseudomonas syringae*. Crystal structures of fully loaded Cu(I)Cu(II) forms. *J. Am. Chem. Soc. 128*, 5834−5850.

(8) Sattler, M., Schleucher, J., and Griesinger, C. (1999) Heteronuclear multidimensional NMR experiments for the structure determination of proteins in solution employing pulsed field gradients. *Prog. Nucl. Magn. Reson. Spectrosc. 34*, 93−158.

(9) Bartels, C., Xia, T. H., Billeter, M., Guntert, P., and Wuthrich, K. (1995) The Program Xeasy For Computer-Supported NMR Spectral-Analysis of Biological Macromolecules. *J. Biomol. NMR 6*, 1−10.

(10) Cornilescu, G., Delaglio, F., and Bax, A. (1999) Protein backbone angle restraints from searching a database for chemical shift and sequence homology. *J. Biomol. NMR 13*, 289−302.

(11) Vuister, G. W., and Bax, A. (1993) Quantitative J Correlation: A New Approach For Measuring Homonuclear 3-Bond $J_{H(N)H(\alpha)}$ Coupling-Constants in N-15-Enriched Proteins. *J. Am. Chem. Soc. 115*, 7772−7777.

(12) Guntert, P. (2004) Automated NMR structure calculation with CYANA. *Methods Mol. Biol. 278*, 353−378.

(13) Schwieters, C. D., Kuszewski, J. J., Tjandra, N., and Clore, G. M. (2003) The Xplor-NIH NMR molecular structure determination package. *J. Magn. Reson. 160*, 65−73.

(14) Laskowski, R. A., Rullmann, J. A. C., MacArthur, M. W., Kaptein, R., and Thornton, J. M. (1996) AQUA and PROCHECK-NMR: Programs for checking the quality of protein structures solved by NMR. *J. Biomol. NMR 8*, 477−486.

(15) Koradi, R., Billeter, M., and Wuthrich, K. (1996) MOLMOL: A program for display and analysis of macromolecular structures. *J. Mol. Graphics 14*, 51−55.

(16) Otwinowski, Z., and Minor, W. (1997) Processing of X-Ray Diffraction Data Collected in Oscillation Mode. *Methods Enzymol. 276*, 307−326.

(17) McCoy, A. J., Grosse-Kunstleve, R. W., Adams, P. D., Winn, M. D., Storoni, L. C., and Read, R. J. (2007) Phaser crystallographic software. *J. Appl. Crystallogr. 40*, 658−674.

(18) Adams, P. D., Afonine, P. V., Bunkóczi, G., Chen, V. B., Davis, I. W., Echols, N., Headd, J. J., Hung, L.-W., Kapral, G. J., Grosse-Kunstleve, R. W., McCoy, A. J., Moriarty, N. W., Oeffner, R., Read, R. J., Richardson, D. C., Richardson, J. S., Terwilliger, T. C., and Zwart, P. H. (2010) PHENIX: A comprehensive Python-based system for macromolecular structure solution. *Acta Crystallogr. D66*, 213−221.

(19) Winn, M., Isupov, M., and Murshudov, G. N. (2001) Use of TLS parameters to model anisotropic displacements in macromolecular refinement. *Acta Crystallogr. D57*, 122−133.

(20) Emsley, P., and Cowtan, K. (2004) Coot: Model-building tools for molecular graphics. *Acta Crystallogr. D60*, 2126−2132.

(21) Davis, I. W., Leaver-Fay, A., Chen, V. B., Block, J. N., Kapral, G. J., Wang, X., Murray, L. W., Arendall, W. B. III, Snoeyink, J., Richardson, J. S., and Richardson, D. C. (2007) MolProbity: All-atom contacts and structure validation for proteins and nucleic acids. *Nucleic Acids Res. 35*, W375−W383.

(22) Vaguine, A. A., Richelle, J., and Wodak, S. J. (1999) SFCHECK: A unified set of procedures for evaluating the quality of macromolecular structure-factor data and their agreement with the atomic model. *Acta Crystallogr. D55*, 191−205.

(23) Vriend, G. (1990) WHAT IF: A molecular modeling and drug design program. *J. Mol. Graphics 8*, 29 , 52−56.

(24) Bertini, I., Luchinat, C., Parigi, G., and Pierattelli, R. (2005) NMR spectroscopy of paramagnetic metalloproteins. *ChemBioChem 6*, 1536−1549.

(25) Olmstead, M. M., Musker, W. K., and Kessler, R. M. (1982) Differences in the coordinating ability of water, perchlorate and tetrafluoroborate toward copper(I). The X-ray crystal structures of $[Cu(1,4\text{-thioxane})_3OClO_3]$, $[Cu(1,4\text{-thioxane})_3OH_2]BF_4$ and $[Cu(1,4\text{-thioxane})_4]BF_4$. *Transition Met. Chem. 7*, 140−146.

(26) Behrens, J., Arnold, S., Klar, G., and Hinrichs, W. (1991) Cyclic ligands with fixed coordination geometry. Part 7. Cationic copper(I) complexes of composition $[Cu(Vn_3S_3)L]^+$-$CF_3SO_3^-$ (Vn_3S_3 = 5,10,15-trithia-cyclo-triveratrylene, L = CO, CH_3OH). *Transition Met. Chem. 16*, 76−81.

(27) Zhou, P., Tian, F., Lv, F., and Shang, Z. (2009) Geometric characteristics of hydrogen bonds involving sulfur atoms in proteins. *Proteins 76*, 151−163.

(28) Robinson, N. J., and Winge, D. R. (2010) Copper metallochaperones. *Annu. Rev. Biochem. 79*, 537−562.

(29) Davis, A. V., and O'Halloran, T. V. (2008) A place for thioether chemistry in cellular copper ion recognition and trafficking. *Nat. Chem. Biol. 4*, 148−151.

(30) Long, F., Su, C. C., Zimmermann, M. T., Boyken, S. E., Rajashankar, K. R., Jernigan, R. L., and Yu, E. W. (2010) Crystal structures of the CusA efflux pump suggest methionine-mediated metal transport. *Nature 467*, 484−488.

(31) Su, C. C., Long, F., Zimmermann, M. T., Rajashankar, K. R., Jernigan, R. L., and Yu, E. W. (2011) Crystal structure of the CusBA heavy-metal efflux complex of *Escherichia coli*. *Nature 470*, 558−562.

(32) Guo, Y., Smith, K., Lee, J., Thiele, D. J., and Petris, M. J. (2004) Identification of methionine-rich clusters that regulate copper-stimulated endocytosis of the human Ctr1 copper transporter. *J. Biol. Chem. 279*, 17428−17433.

(33) De Feo, C. J., Aller, S. G., Siluvai, G. S., Blackburn, N. J., and Unger, V. M. (2009) Three-dimensional structure of the human copper transporter hCTR1. *Proc. Natl. Acad. Sci. U.S.A. 106*, 4237−4242.

(34) Jiang, J., Nadas, I. A., Kim, M. A., and Franz, K. J. (2005) A Mets motif peptide found in copper transport proteins selectively binds Cu(I) with methionine-only coordination. *Inorg. Chem. 44*, 9787−9794.